JACS
JOURNAL OF THE AMERICAN CHEMICAL SOCIETY

ARTICLE

pubs.acs.org/JACS

Tailoring (Bio)chemical Activity of Semiconducting Nanoparticles: Critical Role of Deposition and Aggregation

Irina V. Chernyshova,* Sathish Ponnurangam, and Ponisseril Somasundaran

NSF I/UCRC Center for Particulate & Surfactant Systems (CPaSS), Columbia University, New York, New York 10027, United States

Supporting Information

ABSTRACT: The impact of deposition and aggregation on (bio)chemical properties of semiconducting nanoparticles (NPs) is perhaps among the least studied aspects of aquatic chemistry of solids. Employing a combination of in situ FTIR and ex situ X-ray photoelectron spectroscopy (XPS) and using the Mn(II) oxygenation on hematite (α-Fe_2O_3) and anatase (TiO_2) NPs as a model catalytic reaction, we discovered that the catalytic and sorption performance of the semiconducting NPs in the dark can be manipulated by depositing them on different supports or mixing them with other NPs. We introduce the electrochemical concept of the catalytic redox activity to explain the findings and to predict the effects of (co)aggregation and deposition on the catalytic and corrosion properties of ferric (hydr)oxides. These results offer new possibilities for rationally tailoring the technological performance of semiconducting metal oxide NPs, provide a new framework for modeling their fate and transport in the environment and living organisms, and can be helpful in discriminating between weakly and strongly adsorbed species in spectra.

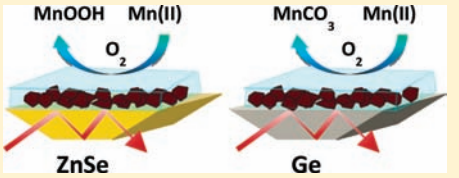

INTRODUCTION

Aquatic chemistry of metal oxide nanoparticles (NPs) in the dark has attracted considerable interest in recent decades due to the large-scale technological applications of such NPs as catalysts, sorbents, sensors, functional coatings, fillers, nanomedical agents, elements of the alternative energy sources, and pigments.[1] The knowledge of the (bio)chemical reactivity of metal oxide NPs is also the key factor in solving a wide range of environmental problems[2,3] and developing eco-friendly methods of assembly, functionalization, and separation of such NPs.[4] Therefore, a mechanistic understanding of how reactivity of these NPs can be rationally controlled is one of the exciting scientific challenges associated with the technological applications.

It is a rule rather than an exception that NPs, without specific ligand-protection, aggregate with themselves or other objects,[5] driven by a reduction in the interfacial free energy of the system. The critical role of (co)aggregation and deposition of semiconducting NPs is well established in photocatalysis.[6,7] However, the impact of these effects on dark aquatic chemistry of semiconducting NPs has mainly eluded the attention of researchers, although there is an emerging understanding of the importance of these effects.[8,9]

We divide the mechanisms by which (co)aggregation and deposition can modify chemical properties of NPs into two categories: extrinsic and intrinsic. The former covers the effects that originate from the aggregate geometry, including the reaction inhibition in the confined space within the aggregates, difference in the exposed crystal faces of the NPs, and competition between different types of NPs for the reactants and products. These effects have previously been invoked to discuss the impact of (co)aggregation on the chemical reactivity of NPs.[8−10] In addition, the regulation phenomenon (electrostatic interaction between two double layers, which results in a change in the surface charge and/or potential of the oxide[11,12]) can also be considered as the external effect.

At the same time, it is well-known that (co)aggregation and deposition can induce changes in the intrinsic, that is, electronic and structural properties of semiconducting NPs, which is the basis for metamaterials design.[13] In particular, the band gap of assembled NPs red shifts with decreasing interparticle separation due to electronic coupling.[14−16] This phenomenon involves Coulomb interaction between the charge carriers and the exchange, or tunneling, interaction between surface atoms belonging to neighboring particles. The exchange interaction modifies the density of states, and eventually results in hybridization, lifting of energetic degeneracy, and leads to delocalization of the states across multiple nanocrystals.[16] The NP distribution also alters interparticle charge transfer[17] due to the local field effects. When two different materials are placed into the ultimate contact, their structures in the interfacial region and orbital occupations are modulated, which underlies the unique electronic, magnetic, and charge transport properties of transition metal oxide heterostructures,[18] along with the diffusional ion intermixing.[19] However, these effects have been ignored in past studies of dark chemistry of semiconducting NPs.

Herein, we show that (i) changes in the electronic properties is the main driving force of the effects of (co)aggregation and deposition on the catalytic activity of semiconducting metal oxide NPs and (ii) a mechanistic understanding of these effects calls for a shift from the common chemical to emerging electrochemical paradigm for the dark reactivity of these NPs.

Received: March 11, 2011
Published: May 10, 2011

dx.doi.org/10.1021/ja202266g | J. Am. Chem. Soc. 2011, 133, 9536–9544

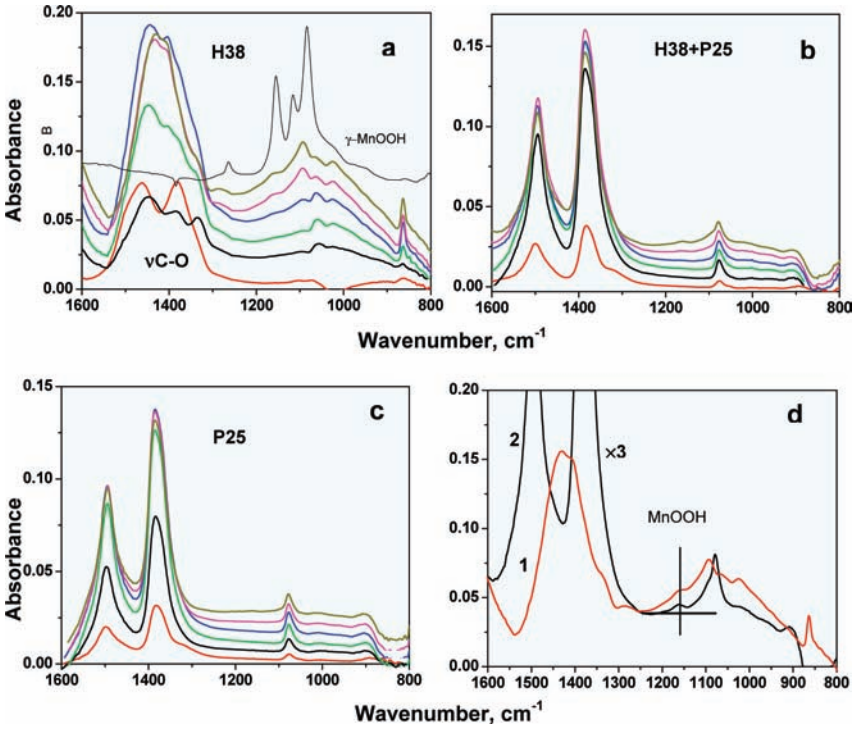

Figure 1. Time-dependent in situ FTIR spectra of NPs deposited on ZnSe: (a) 38 nm hematite (H38), (b) 1:2 mixture (by weight) of H38 and 30 nm titania (P25), and (c) P25 reacting with a 27 ppm Mn(II) solution in a 10^{-2} M bicarbonate buffer at pH 8.55. The bottom spectrum was measured 2−3 min after adding Mn(II). Time interval between the spectra was 1 h. Time increases from bottom (red) to top spectrum. Diffuse reflectance spectrum of dry synthetic γ-MgOOH is shown for comparison in (a). All spectra are offset for better clarity. (d) Comparison of spectra of (1) 38 nm hematite and (2) 1:2 mixture of 38 nm hematite and P25 titania reacted for 5 h. The spectrum of the mixture was multiplied by 3 to normalize to the same effective mass.

As a model redox reaction, we study the Mn(II) catalytic oxygenation:

$$Mn^{2+} + 1/4O_2 + 3/2H_2O \rightarrow MnOOH + 2H^+ \qquad (A)$$

by hematite (α-Fe_2O_3) and anatase NPs. This reaction is an important environmental process,[20] which is extremely slow at pH < 8.5 if it proceeds homogeneously.[21] It can be used as a prototype for the scavenging of heavy metals, radionuclides, and redox-unstable pollutants by naturally occurring ferric (hydr)oxide NPs. Such NPs are ubiquitous in the environment (oceans, ground and surface waters, sediments, dust, soils, and acid mine drainage), where they participate in many (bio)geochemical processes including sinking of atmospheric carbon dioxide, metabolism of bacteria, and supplying of nutrients to plants and phytoplankton. Ferric (hydr)oxide and titania NPs are among the most popular industrial sorbents, pigments, fillers, and catalysts. Ferric (hydr)oxides have a great potential to enlarge their segment as compared to titania due to relatively low cost, nontoxicity, and environmentally benign character.

MATERIALS AND METHODS

Highly monodisperse and pure hematite NPs with mean sizes of 38 and 9 nm were synthesized by forced hydrolysis. P25 TiO_2 NPs (81% anatase and 19% rutile) were acquired from Nippon Aerosil (Evonik). The NPs were characterized by a wide range of techniques, including TEM, XRD, Raman spectroscopy, XPS, BET surface area, titration, and electrokinetic measurements. The synthesis procedures and the characterization of the NPs can be found in the Supporting Information.

In situ FTIR spectroscopic measurements were performed in the horizontal attenuated total reflection (HATR) geometry using a Perkin-Elmer Spectrum 100 FTIR spectrometer equipped with an MCT detector and a HATR accessory. Two HATR cells with ZnSe and Ge internal reflection elements (IRE) (10 internal reflections, angle of incidence 45°), respectively, covered by caps to prevent evaporation of water were employed. The IREs were coated with NPs at a surface density of ~7 mg/cm^2. To determine the oxidation state of adsorbed Mn(II) as well as to quantify the Mn(II) adsorption density, samples collected after the in situ FTIR experiments were analyzed by XPS. UV−vis absorption spectroscopy was used to monitor the effects of (co)aggregation on the band gap of hematite and titania NPs. Full technical details of the FTIR, XPS, and UV−vis measurements are provided in the Supporting Information.

RESULTS

To understand the effects of (co)aggregation and deposition on the catalytic activity of hematite NPs, we compare kinetics of reaction (A) catalyzed by (i) 38 and 9 nm hematite NPs alone and in the 1:2 mixture by weight with 30 nm titania NPs, (ii) by 30 nm titania and 38 nm hematite alone, as well as by (iii) 38 nm hematite NPs alone deposited on different (ZnSe and Ge) supports. Because of similar packing of the deposited NPs, this experimental design allows one to exclude the extrinsic effects from the main causes of the observed variations in the catalytic performance. We use in situ FTIR spectroscopy to monitor the formation of the reaction products as a function of time. The reaction products are additionally analyzed ex situ using XPS.

The initial product of the Mn(II) oxygenation on 38 nm hematite NPs deposited alone on ZnSe (Figure 1a) is characterized by two main absorption bands at ~1465 and 1380 cm^{-1} and two weak bands at 1060 and 860 cm^{-1}, assignable to $MnCO_3$

dx.doi.org/10.1021/ja202266g |J. Am. Chem. Soc. 2011, 133, 9536–9544

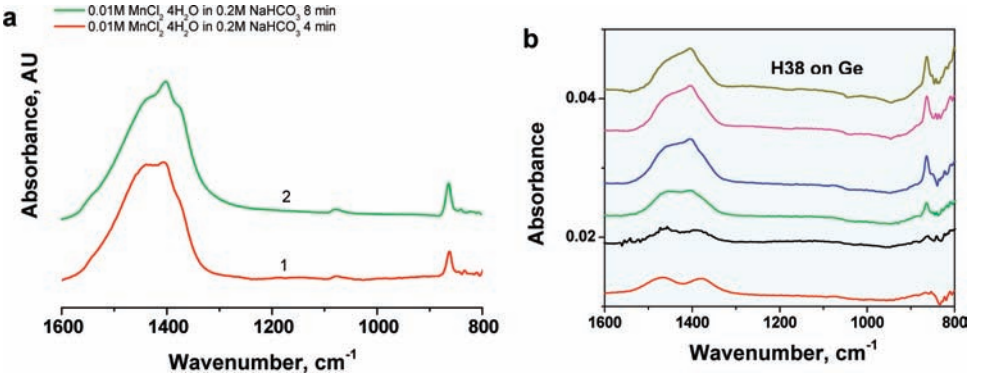

Figure 2. (a) HATR spectra of a $MnCO_3 \cdot nH_2O$ precipitate formed by adding 0.01 M $MnCl_2 \cdot 4H_2O$ to 0.2 M $NaHCO_3$ after (1) 4 min and (2) 8 min of aging. (b) Time-dependent in situ FTIR spectra of 38 nm hematite NPs deposited on Ge in a 27 ppm Mn(II) solution in a 10^{-2} M bicarbonate buffer at pH 8.55. The bottom spectrum was measured 2−3 min after adding Mn(II) into the FTIR cell. Time interval between the spectra was 1 h. Time increases from bottom (red) to top spectrum. All spectra are offset for better clarity.

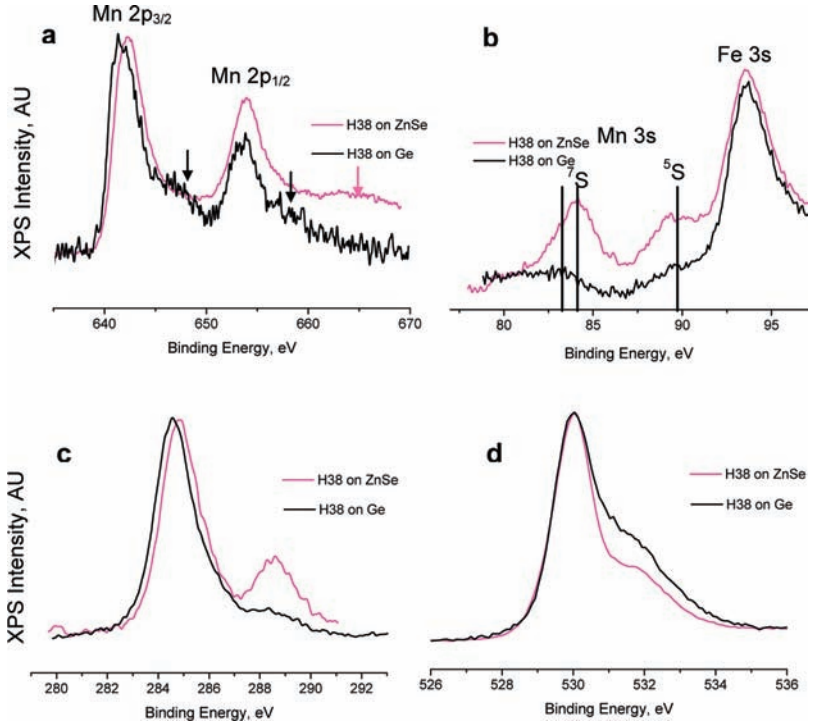

Figure 3. XPS core-level (a) Mn 2p, (b) Mn 3s, (c) C 1s, and (d) O 1s spectra of 38 nm hematite after reaction with 27 ppm Mn(II) in 0.01 M $NaHCO_3$ at pH 8.55 in the in situ FTIR cell, after measuring spectra shown in Figures 1a and 2b, respectively. The M_n 2p satellites are shown by arrows.

(Figure 2a). With elapse of time, a new set of absorption bands at 1025, 1093, and 1155 cm^{-1} appears and further increases in intensity. On the basis of spectral similarities, these bands are attributed to the bending δMn−OH modes of manganite (γ-MnOOH). The XPS analysis confirms this interpretation (vide infra). Similar spectral dependences on time are observed upon varying the solution conditions (Figure S4) as well as for 9 nm hematite (Figure S5a). However, when 38 nm hematite is deposited on Ge, the reaction does not propagate, as evidenced by the absence of the characteristic γ-MnOOH bands in the 1000−1200 cm^{-1} region (Figure 2b). Hence, in contact with Ge, hematite NPs lack their ability to catalyze reaction (A).

The 38 nm hematite NPs reacted with Mn(II) as deposits on the ZnSe and Ge crystals were further analyzed using XPS. The Mn/Fe atomic ratio of 18% and 6% for ZnSe and Ge, respectively, indicates that Ge lowers sorption capacity of the deposited NPs. Comparison of the Mn 2p photoemission spectra (Figure 3a) shows that in the case of Ge the Mn $2p_{3/2}$ and Mn $2p_{1/2}$ spin−orbit components at about 642 and 653 eV, respectively, are at lower binding energies and their branching ratio (a ratio of the Mn $2p_{3/2}$ to Mn $2p_{1/2}$ peak areas) is higher. This spectral picture suggests that the mean oxidation state of the adsorbed manganese is lower in the case of Ge.[22]

More information can be extracted from the analysis of the Mn 2p satellites at ~648 and 664 eV. These satellites are generated by a charge transfer from the ligand state to the 3d metal state and hence are sensitive to the oxidation state of manganese.[22−24] Separation of the satellites from the main peaks decreases while

dx.doi.org/10.1021/ja202266g |J. Am. Chem. Soc. 2011, 133, 9536–9544

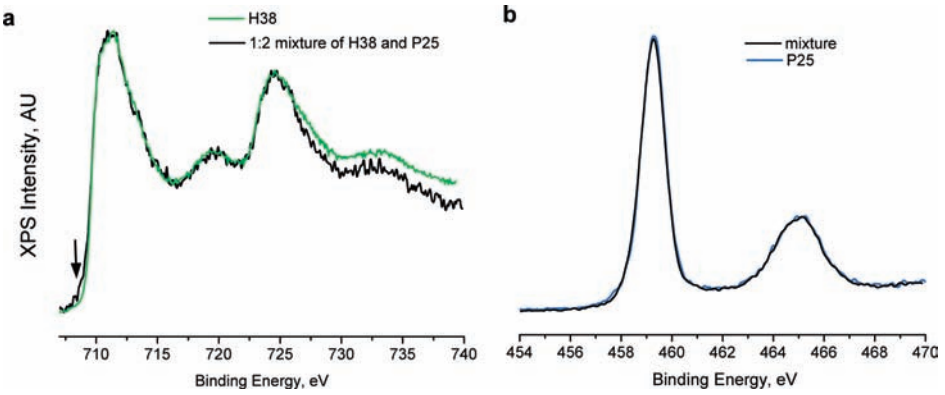

Figure 4. XPS (a) Fe 2p and (b) Ti 2p spectra of a 1:2 mixture of H38 with P25 in comparison with the corresponding spectra of NPs alone. Arrow shows a shoulder due to reduced ferric ions.

the satellite intensity increases with increasing formal 3d occupation of manganese. As a result, a prominent Mn $2p_{3/2}$ satellite is typical for Mn(II)-containing compounds.[22,23,25] However, this satellite is hardly distinguishable for Mn(III) and Mn(IV) (hydr)oxides due to its overlap with the Mn $2p_{1/2}$ main peak.[23,26,27] In contrast, the Mn $2p_{1/2}$ satellite is common for Mn(III) and Mn(IV) (hydr)oxides.[23,27] As seen from Figure 3a, the Mn $2p_{1/2}$ peak of the ZnSe-supported sample is accompanied by the charge transfer satellite shifted by 10.2 eV, which is close to 10−10.5 eV reported[23,28] for Mn_2O_3 and Mn_3O_4, while the Mn $2p_{3/2}$ satellite is missing. In contrast, the Ge-supported sample is characterized by the Mn $2p_{3/2}$ satellite with a binding energy shift of 4.7 eV, which is comparable with 4.9 eV measured[23] for MnO. The Mn $2p_{1/2}$ satellite of this sample overlaps the high binding energy side of the main Mn $2p_{1/2}$ peak (shown by arrow). Hence, Mn(III) is present on the surface of the ZnSe-supported NPs, while Mn(II) dominates on the Ge-supported NPs.

The above result agrees with the $^5S-^7S$ multiplet splitting in the Mn 3s core-level spectra. This splitting is commonly more sensitive to the Mn oxidation state as compared to the Mn 2p photoemission, increasing with increasing the formal 3d occupation of manganese ions.[22,28−31] The Mn 3s spectra of the Ge- and ZnSe-supported NPs show the multiplet splitting of 6.3 and 5.9 eV, respectively (Figure 3b). Taking into account the multiplet splitting of 6.2 eV for rhodocrosite ($MnCO_3$),[31] MnO,[28] and manganese ferrite ($MnFe_2O_4$),[24] 5.6 eV for Mn_3O_4,[28] and 5.4−5.3 eV for manganate (γ-MnOOH) and Mn_2O_3,[30,31] one can conclude that the average oxidation state of Mn on the Ge- and ZnSe-supported NPs is +2 and +2.3, respectively. (The latter value is obtained using the valence state correlation shown in Figure S8.)

The Fe 2p spectrum of 38 nm hematite (Figure 4a) is typical of that of well-crystalline hematite, exhibiting shakeup satellite, phonon broadening, and multiplet splitting in the final state.[32] When these NPs are mixed with P25 titania, a weak shoulder appears at lower binding energies (marked by arrow), which suggests that the hematite NPs are partially reduced. We did not succeed in acquiring XPS spectra of the titania NPs and the hematite−titania mixtures that interacted with Mn because these samples exhibit a strong charging effect during the spectrum acquisition, which we unable to eliminate by adjusting settings of the electron flood gun.

Finally, FTIR spectra obtained for NPs deposited on ZnSe demonstrate that, in contrast to the hematite NPs, P25 titania NPs do not catalyze the reaction: The spectra of reacted P25 exhibit only the carbonate manifold (Figure 1c). Furthermore, when 38 or 9 nm hematite NPs are mixed with P25 titania in a 1:2 ratio by weight, reaction (A) slows by a factor of ∼2 and ∼3.5, respectively, as compared to the corresponding hematite NPs alone. This conclusion is based on comparison of the amounts of manganite in the final products evaluated based on the scaled intensity of the manganite peak at ∼1160 cm^{-1} (Figures 1b and S5c). To scale the spectrum intensity, we assumed that the reaction is catalyzed only by hematite NPs while titania NPs are inert in the mixture. On the basis of this assumption, we multiplied the peak intensity of the manganate band by a factor of 3 (the mass fraction of the hematite NPs in the mixtures).

DISCUSSION

The remarkable impact of coaggregation, deposition, and composition of the transition metal oxide NPs on their catalytic performance can be understood by considering the electronic properties of the composites in comparison with the NPs alone. Moreover, the observed regularities allow the clarification of the mechanism of the catalytic reaction (A).

Change in the Electronic Properties of Hematite NPs upon Coaggregation and Deposition. Before explaining the reasoning behind these statements, we will consider the effects caused by the electrical contact of two different ideal n-type semiconductors with different energies of the Fermi levels (the electrochemical potentials of electrons), E_F. The contact requires electron transfer (ET) between the semiconductors until E_F at both sides of the interface are equilibrated. However, this can only be accomplished provided the conduction bands of these semiconductors overlap because no electronic states are available in the forbidden energy gap of the semiconductors. The extent of this process further depends on the carrier densities at the semiconductor surfaces. As seen from the relative energies of the conduction bands (Figure 5), both n-type Ge and TiO_2 can readily inject electrons into hematite. The electron enrichment of hematite NPs mixed with titania is indeed observed by XPS (Figure 4a), while the conjugated electron depletion of titania is evidenced by the red shift of the absorption edge of these NPs in their mixtures with hematite (Figure S6a).

Germanium is expected to inject electrons more efficiently than TiO_2 because undoped Ge has much higher conductivity (∼10^{-2} vs ∼10^{-6} S cm^{-1}) due to the narrow bandgap of only 0.66 eV and hence the high concentration of thermally excited free electrons. In addition, energies of the conduction bands of Ge and α-Fe_2O_3 are closer to each other. This is important given

dx.doi.org/10.1021/ja202266g |J. Am. Chem. Soc. 2011, 133, 9536–9544

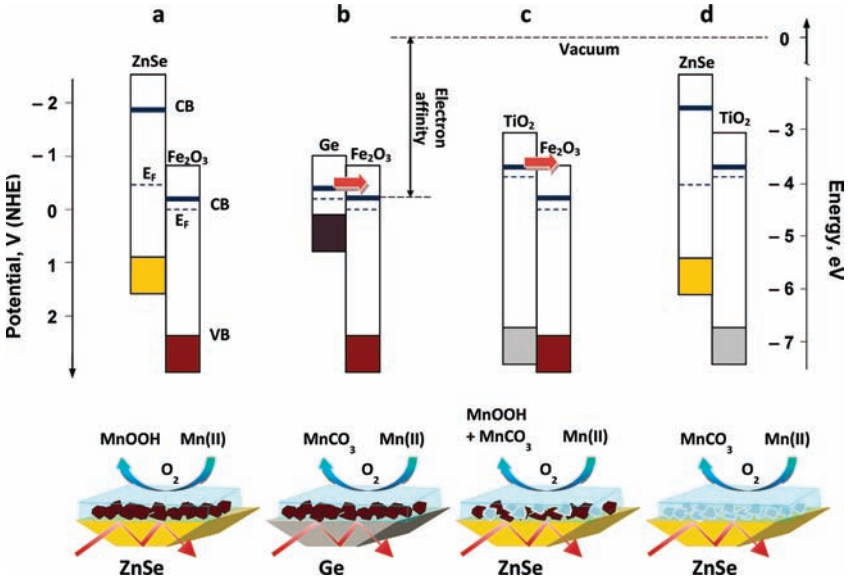

Figure 5. Schematic explanation of the effects of coaggregation and deposition on electronic properties of hematite NPs contacted at pH 8.55 with (a) ZnSe, (b) Ge, and (c) 30 nm anatase. (d) Energy spectrum of 30 nm anatase deposited on ZnSe. CB and VB = conduction and valence band, respectively, E_F = Fermi level. Positions of the band edge and Fermi levels are extrapolated from refs 33−36 assuming their Nernstian behavior.

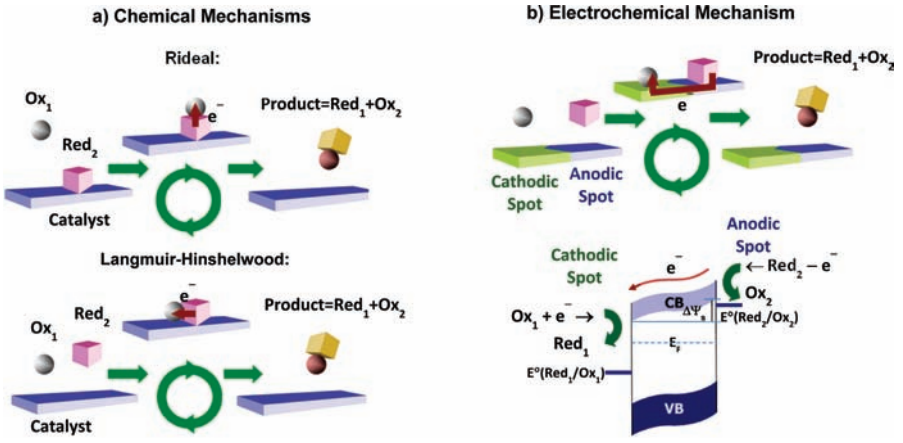

Figure 6. Conceptual schemes of (a) chemical and (b) electrochemical mechanisms of a heterogeneous catalysis of redox reaction $Ox_1 + Red_2 \rightarrow Red_1 + Ox_2$. Chemical mechanism is shown as Rideal type (an oxidant Ox_1 reacts from solution with adsorbed reductant Red_2) as well as Langmuir−Hinshelwood type (charge transfers between two proximate adsorbates Red_2 and Ox_1). Electrochemical mechanism is shown for n-type semiconductor with heterogeneous surface having anodic and cathodic spots. $\Delta\Psi_s$ = gradient of potential, VB = valence band, CB = conduction band. Wine-color arrows show the ET path.

the narrow (∼1 eV) width of the conduction band of hematite caused by the strong localization of its Fe 3d electrons.[37] At the same time, the extremely low conductivity of undoped ZnSe ($\sim 10^{-11}$ S cm^{-1}) coupled with the absence of an effective overlap of its conduction band ZnSe with that of hematite (Figure 5a) makes ZnSe electronically inert with respect to hematite. Thus, hematite NPs are negatively charged in contact with Ge or titania as compared to ZnSe due to the Fermi-level equilibration, the effect being more pronounced in the case of Ge.

Mechanism of the Catalytic Activity. The paradigm long-held for aquatic chemistry of metal oxide NPs in the dark[3,38] can be called chemical as it neglects both the semiconducting properties of the NPs and the long-distance charge transfer within the NP. Specifically, in the case of heterogeneous catalysis, the chemical mechanism implies that both the oxidation and the reduction half-reactions of a redox reaction $Ox_1 + Red_2 \rightarrow Red_1 + Ox_2$ take place at the same site, or at two nearest-near neighbor adsorption sites, although the details can vary (Figure 6a). The kinetics of ET in such a process is determined by the relative positions of the HOMO and LUMO of the reactants. The catalytic effect of the surface is attributed to accumulating the reactants and decreasing the activation energy for ET.[39] In particular, oxygenation is believed to be facilitated by the adsorption-induced increase of electron density on the reducing species, which decreases the formal reduction potential of the adsorbate and thus makes this species more prone to electrophilic attack.[3,20,40,41] Hence, if the chemical paradigm were valid, the electron enrichment of hematite NPs either by depositing on Ge or mixing with titania would accelerate the rate of the Mn(II) oxygenation as compared to the hematite NPs deposited on

dx.doi.org/10.1021/ja202266g |*J. Am. Chem. Soc.* 2011, 133, 9536–9544

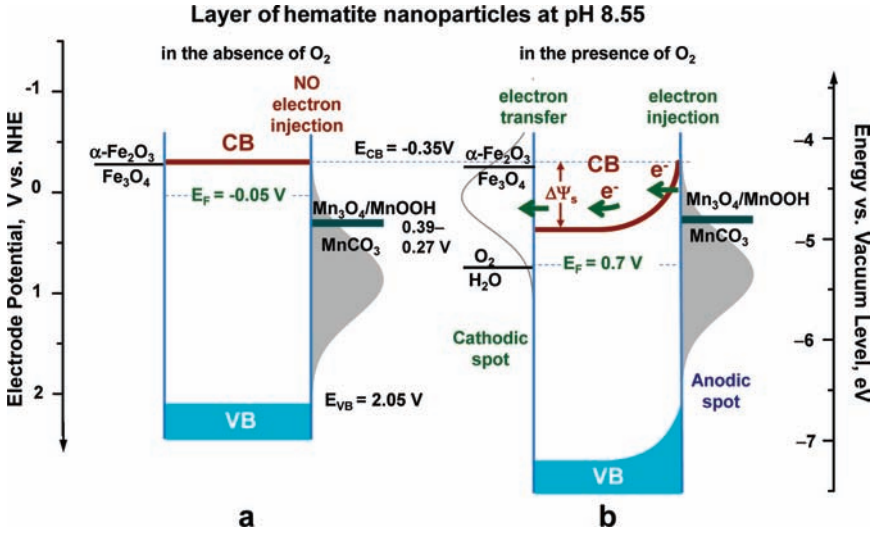

Figure 7. Schematic diagram of the interfacial energetics of hematite layer at pH 8.55 (a) in the absence of dissolved oxygen and (b) under air-saturated conditions after addition of Mn(II) to the solution. VB = valence band, CB = conduction band. Shaded and empty Gaussians depict distributions of filled and empty electron levels of dissolved Mn(II) and O_2, respectively, with a typical reorganization energy of 1 eV.[51]

ZnSe, which is contrary to what is observed. Also, the chemical paradigm is unable to account for the catalytic inertness of titania NPs. On this basis, we discard this paradigm.

A specific feature of the alternative, that is, electrochemical pathway is spatial separation of the oxidation and reduction half-reactions, which are electrically coupled by charge transfer within the catalyst (Figure 6b). This can happen provided the free-energy change is negative at each of the three steps (electron injection from the reductant, electron drift from the anodic to cathodic spot within the semiconductor, and ET to the oxidant). Because ET across the semiconductor−electrolyte interface is energy conserving (Franck−Condon principle) and occurs only through a narrow distribution of energies near the bottom of the conduction band edge at the interface E_{CB},[42,43] the distributions of the filled and empty energy levels of both the reductant and the oxidant must match, in the case of n-type semiconductor, positions of the conduction band at the anodic and cathodic spots, respectively. Finally, the product of the surface potential drop, $\Delta\Psi_s$, and the NP conductivity should be sufficient to support ET between the anodic and cathodic reaction spots.

As different from the chemical paradigm, the electrochemical mechanism takes into consideration the semiconductor side of the electric double layer through incorporating new variables such as energies of electrons and holes, the position of the Fermi level relative to the conduction and valence band edges at the semiconductor surface, the rectifying properties of the space charge layer, and conductivity of the semiconductor. The electrochemical mechanism is generally accepted for adsorption and catalytic reactivity of semiconducting sulfides in the dark[44−47] and, as we show below, offers simple interpretation of our results.

Reaction (A) is split into the oxidation and reduction half-reactions as

$$\equiv S-MnCO_{3ads} + 2H_2O \rightarrow \equiv S-MnOOH_{ads} + CO_3^{2-} + 3H^+ + e \quad (B)$$

and

$$O_2 + 4e + 4H^+ \rightarrow 2H_2O \quad (C)$$

respectively, where e denotes electron, although the actual pathways can include several intermediate steps.

The thermodynamic feasibility of electronic coupling of process (B) to process (C) through a layer of 38 nm hematite NPs can be inferred on the basis of the general electrochemical concept of the charge transfer between a semiconductor and a solution[42,43,48] and the bulk thermodynamic data for half-reactions (B) and (C).[49,50] The layer is characterized by the band gap of ∼2.4 eV (Figure S7). Its other electronic properties are assumed to be, as a first approximation, similar to those of a polycrystalline hematite electrode,[36] that is, n-type conductivity due to O-vacancies, the flat band potential (the electrode potential at which the potential drop across the space charge layer is zero), E_{fb}, of −0.05 V (NHE) at pH 8.55, and energy gap of 0.3 eV between E_F and bottom of conduction band E_{CB}. As seen from Figure 7a, in the absence of redox active species in the solution, the hematite layer attains its flat band potential because there are no available levels for charge transfer between its interior and the solution. Under these conditions, Mn(II) ions cannot be oxidized by hematite because the redox potential of the $MnOOH/MnCO_3$ couple of ∼0.45 V is higher than E_F of the oxide.

The situation is essentially different in the presence of dissolved O_2 (Figure 7b). Oxygen will preferably be adsorbed on the most negatively charged facets or surface sites of the hematite layer and can further be reduced[52] because the necessary conditions for this reaction are satisfied. In fact, the potential of half-reaction (C) is below E_F, while the electron level distribution of dissolved O_2 in the solution overlaps with the conduction band of hematite. Hence, free electrons will be consumed by oxygen, and a depletion region will appear at the surface of the semiconductor. In the steady state, hematite will be charged positively attaining the potential of half-reaction (C). The resulting downward shift of E_F places it below the $MnOOH/MnCO_3$ redox potential at the interface, making the electron injection from Mn(II) to the conduction band thermodynamically allowed. Because the $MnOOH/MnCO_3$ redox potential in the energy diagram is below E_{CB}, we speculate that surface states mediate this act, tunneling across the interfacial barrier takes

dx.doi.org/10.1021/ja202266g | J. Am. Chem. Soc. 2011, 133, 9536–9544

place, or the reaction is accomplished by holes. If injected, the electron will be moved away by the potential drop in the space charge layer $\Delta\Psi_s$ from the anodic spot toward the cathodic spot where an O_2 molecule can consume it (Figure 7b). Therefore, the net reaction (A) can proceed through the electrochemical route.

Cathodic polarization of a semiconductor (in our case, negative charging of the hematite layer by electrons transferred from Ge or titania) shifts its E_F upward. The resulting reduction of the driving force of electron injection into the semiconductor, along with a smaller potential drop $\Delta\Psi_s$, slows reaction (A). Furthermore, high energies E_{CB} and E_F of TiO_2 exclude the anodic half-reaction (B) on these NPs, which can be a rationale for the lack of the catalytic activity by P25 NPs. Finally, the above reasoning suggests that the oxidation half reaction is the rate-determining step, while the alternative reaction routes such as the Mn(II) oxygenation by peroxide species created either during the O_2 reduction or the Fenton process are unlikely.

Thus, given similarities in the electronic properties of ferric (hydr)oxides,[53] we arrive at the conclusion that aquatic chemistry of such NPs in the dark can be affected by charge equilibration with other semiconductors or metals, similar to the well-known case of photoexcited semiconductor nanoparticles.[6,54] Moreover, changes in the intrinsic (normalized by the effective surface area of the NPs in suspensions) oxidative catalytic activity of ferric (hydr)oxide NPs by the contact phenomena can a priori be predicted on the basis of the reported electron energy characteristics of solids.[55−57] Specifically, combinations with semiconductors characterized by higher E_{CB} and E_F energies (e.g., TiO_2, ZnO, CdS, and Ge) or with metals that have low work functions (e.g., Fe, Cr, Ti, Al, and V) are expected to suppress the intrinsic oxidative catalytic activity of hematite NPs. At the same time, CuO, V_2O_3, In_2O_3, WO_3, CdO, Ni, Au, Pt, and Pd will promote this activity. Indeed, the Au/α-Fe_2O_3 nanoparticulate gas catalysts demonstrate advanced oxidative catalytic properties as compared to hematite NPs alone.[58]

The electrochemical concept also predicts that the intrinsic oxidative catalytic activity of ferric (hydr)oxide NPs is improved by aggregation. In fact, as seen from UV−vis spectra of 38 nm hematite NPs in the different aggregation states [Figure S6b and text of Supporting Information], the band gap of the aggregates decreases when increasing their size. This effect, explained by the interparticle electron coupling, is typical for semiconducting NPs.[15,16,59] Because aggregation shifts the E_{CB} energy of semiconducting NPs downward,[15,16,59] their electron affinity increases (defined as the energy difference between the vacuum level and the bottom of the conduction band as depicted in Figure 5). This effect results in better electron coupling of the conduction band with filled electronic levels of the reductant. An additional effect that increases the reaction rate in larger aggregates is due to a larger potential drop in their space charge layer, which improves charge refinement[7] and hence speeds up charge transfer between the anodic and cathodic spots.

Another practically important effect to consider is the reduction of ferric (hydr)oxides. According to the E−pH Pourbaix diagram,[49] cathodic polarization converts hematite into magnetite at pH > 7:

$$3Fe_2O_3 + 2H^+ + 2e \rightarrow 2Fe_3O_4 + H_2O \qquad (D)$$

while at a lower pH hematite dissolves with releasing ferrous ions into the solution. As seen from Figure 7 and following from the above consideration, the aggregation-induced downward shift of E_{CB} will inhibit reaction (D). Given the hematite band gap is due to the O 2p−Fe 3d charge transfer,[53] its closing can be related to the enhancement of the O 2p−Fe 3d hybridization by the aggregation-induced increase in electron coupling, which suggests that the Fe−O bonds are stabilized in the aggregates. The quenching of proton-assisted dissolution of aggregated goethite NPs at acidic pH under anaerobic conditions[9] corroborates this conclusion.

Strong support for the suggested electrochemical mechanism is provided by past studies of the Fe(II) adsorption on ferric (hydr)oxides in the absence of oxygen.[60−62] Specifically, it was established that adsorbed Fe(II) ions inject electrons into the Fe(III) oxide NPs[60] and single crystals,[62] this reaction being coupled to the reductive dissolution of the Fe(III) oxide at remote sites. In addition, it was demonstrated that such a process is maintained by an electric current between the facets of a hematite crystal.[61] At the same time, electrons are not removed from Fe(II) adsorbed on TiO_2 and Al_2O_3.[60] However, none of the cited studies invokes the electrochemical concept and terminology for interpreting their findings. Also, none considers the electronic structure of the semiconducting metal oxides as the fundamental precause of the effects observed. Moreover, these studies are limited to a simpler case of the Fe(II) oxidation by the Fe(III) oxide itself, which is not a catalytic reaction.

Finally, the found dependence of the sorption capacity of semiconducting NPs on the electronic properties of the support can be helpful in discriminating contributions of weakly and strongly adsorbed species in complex spectra of the reacted NPs. Moreover, this phenomenon suggests that care must be taken when in situ FTIR-ATR spectroscopy results obtained using different IRE crystals are compared one to another.

CONCLUSIONS

Catalytic activity of hematite NPs for the Mn(II) oxygenation degrades when the NPs are mixed with P25 titania. Hematite and P25 titania NPs deposited alone on Ge and ZnSe, respectively, do not catalyze the reaction, while sorption capacity of hematite NPs decreases. These findings are consistent with the electrochemical pathway where the anodic and cathodic half-reactions are reactions (B) and (C), respectively, reaction (B) being the rate-determining step. The decisive role in the effects of (co)aggregation and deposition is played by changes in the electronic properties (such as electrochemical potential, energy gap, energy of the conduction and valence bands, and the potential drop in the space charge layer) of the semiconducting NPs due to the contact phenomena. These changes are expected to be accompanied by structural transformations of the NPs. The results of our study represent the first steps to the rational control of dark (bio)chemical activity of such NPs through the (co)aggregation and deposition effects by selecting different electronic configurations of the contacting phases.

ASSOCIATED CONTENT

Supporting Information. Synthesis details for hematite NPs, the technical details of the physic-chemical methods, X-ray diffractograms, Raman spectra, TEM images, BET surface areas, points of zero charge (PZC), and isoelectric point (IEP) of the NPs; time-dependent in situ FTIR spectra of the Mn(II) adsorption on (a) 38 nm hematite at pH 8 and 9 as well as (b)

9 nm hematite and its 1:2 mixture with P25 at pH 8.55; UV−vis spectra showing the effects of (co)aggregation on the band gaps of P25 and 38-nm hematite; a Tauc−Mott plot for direct band gap of 38 nm hematite, and a plot of the Mn oxidation state versus Mn 3s multiplet splitting. This material is available free of charge via the Internet at http://pubs.acs.org.

AUTHOR INFORMATION

Corresponding Author
irina905c@gmail.com

ACKNOWLEDGMENT

Support from the NSF under grant nos. 0925232, UCSB KK9157, and 0749461 as well as from the Tata Research Development and Design Center, Pune, India, is acknowledged. We also thank Prof. Nick Turro and anonymous reviewers for useful suggestions. This work used the shared experimental facilities that are supported primarily by the MRSEC program of NSF #DMR 0213574 and by the New York State Office of Science Technology and Academic Research (NYSTAR).

REFERENCES

(1) Richards, R. M. In *Dekker Encyclopedia of Nanoscience and Nanotechnology*; Schwarz, J. A., Contescu, C. I., Putyera, K., Eds.; Marcel Dekker, Inc.: New York, 2004.
(2) *Nanotechnologies for Water Environment Applications*; Zhang, T. C., Surampalli, R. Y., Lai, K. C. K., Hu, Z., Tyagi, R. D., Lo, I. M. C., Eds.; American Society of Civil Engineers: Reston, VA, 2009.
(3) Stumm, W.; Morgan, J. J. *Aquatic Chemistry*, 3rd ed.; Wiley: New York, 1996.
(4) Jolivet, J. P.; Cassaignon, S.; Chaneac, C.; Chiche, D.; Durupthy, O.; Portehault, D. *C. R. Chim.* **2010**, *13*, 40.
(5) Petosa, A. R.; Jaisi, D. P.; Quevedo, I. R.; Elimelech, M.; Tufenkji, N. *Environ. Sci. Technol.* **2010**, *44*, 6532.
(6) Serpone, N.; Maruthamuthu, P.; Pichat, P.; Pelizzetti, E.; Hidaka, H. *J. Photochem. Photobiol., A* **1995**, *85*, 247.
(7) Lakshminarasimhan, N.; Kim, W.; Choi, W. *J. Phys. Chem. C* **2008**, *112*, 20451.
(8) Liu, J.; Aruguete, D. M.; Murayama, M.; Hochella, M. F. *Environ. Sci. Technol.* **2009**, *43*, 8178.
(9) Rubasinghege, G.; Lentz, R. W.; Park, H.; Scherer, M. M.; Grassian, V. H. *Langmuir* **2010**, *26*, 1524.
(10) Bose, S.; Hochella, M. F.; Gorby, Y. A.; Kennedy, D. W.; McCready, D. E.; Madden, A. S.; Lower, B. H. *Geochim. Cosmochim. Acta* **2009**, *73*, 962.
(11) Kallay, N.; Preocanin, T.; Kovacevic, D. *Croat. Chem. Acta* **2009**, *82*, 531.
(12) Lyklema, J.; Duval, J. F. L. *Adv. Colloid Interface Sci.* **2005**, *114*, 27.
(13) Urban, J. J.; Talapin, D. V.; Shevchenko, E. V.; Kagan, C. R.; Murray, C. B. *Nat. Mater.* **2007**, *6*, 115.
(14) Yu, H. T.; Liu, Y.; Brock, S. L. *ACS Nano* **2009**, *3*, 2000.
(15) Dollefeld, H.; Weller, H.; Eychmuller, A. *J. Phys. Chem. B* **2002**, *106*, 5604.
(16) Zhang, J. H.; Lutich, A. A.; Susha, A. S.; Doblinger, M.; Mauser, C.; Govorov, A. O.; Rogach, A. L.; Jackel, F.; Feldmann, J. *J. Appl. Phys.* **2010**, *107*, 123516.
(17) Hendry, E.; Koeberg, M.; O'Regan, B.; Bonn, M. *Nano Lett.* **2006**, *6*, 755.
(18) Pentcheva, R.; Pickett, A. E. *J. Phys.: Condens. Matter* **2010**, *22*, 043001.
(19) Chambers, S. A.; Engelhard, M. H.; Shutthanandan, V.; Zhu, Z.; Droubay, T. C.; Qiao, L.; Sushko, P. V.; Feng, T.; Lee, H. D.; Gustafsson, T.; Garfunkel, E.; Shah, A. B.; Zuo, J. M.; Ramasse, Q. M. *Surf. Sci. Rep.* **2010**, *65*, 317.
(20) Davies, S. H. R.; Morgan, J. J. *J. Colloid Interface Sci.* **1989**, *129*, 63.
(21) Diem, D.; Stumm, W. *Geochim. Cosmochim. Acta* **1984**, *48*, 1571.
(22) Nelson, A. J.; Reynolds, J. G.; Roos, J. W. *J. Vac. Sci. Technol., A* **2000**, *18*, 1072.
(23) Oku, M.; Hirokawa, K.; Ikeda, S. *J. Electron Spectrosc. Relat. Phenom.* **1975**, *7*, 465.
(24) Allen, G. C.; Harris, S. J.; Jutson, J. A.; Dyke, J. M. *Appl. Surf. Sci.* **1989**, *37*, 111.
(25) Beyreuther, E.; Grafstrom, S.; Eng, L. M.; Thiele, C.; Dorr, K. *Phys. Rev. B* **2006**, *73*, 155425.
(26) Uozumi, T.; Okada, K.; Kotani, A.; Zimmermann, R.; Steiner, P.; Hufner, S.; Tezuka, Y.; Shin, S. *J. Electron Spectrosc. Relat. Phenom.* **1997**, *83*, 9.
(27) Dicastro, V.; Polzonetti, G. *J. Electron Spectrosc. Relat. Phenom.* **1989**, *48*, 117.
(28) Galakhov, V. R.; Demeter, M.; Bartkowski, S.; Neumann, M.; Ovechkina, N. A.; Kurmaev, E. Z.; Logachevskaya, N. I.; Mukovskii, Y. M.; Mitchell, J.; Ederer, D. L. *Phys. Rev. B* **2002**, *65*, 113102.
(29) Fujiwara, M.; Matsushita, T.; Ikeda, S. *J. Electron Spectrosc. Relat. Phenom.* **1995**, *74*, 201.
(30) Nelson, A. J.; Reynolds, J. G.; Christou, G. *J. Appl. Phys.* **2003**, *93*, 2536.
(31) Junta, J.; Hochella, M. F. *Geochim. Cosmochim. Acta* **1994**, *58*, 4985.
(32) McIntyre, N. S.; Zetaruk, D. G. *Anal. Chem.* **1977**, *49*, 1521.
(33) Kavan, L.; Gratzel, M.; Gilbert, S. E.; Klemenz, C.; Scheel, H. J. *J. Am. Chem. Soc.* **1996**, *118*, 6716.
(34) Huygens, I. M.; Strubbe, K. *J. Electrochem. Soc.* **2008**, *155*, F49.
(35) Gautron, J.; Lemasson, P.; Rabago, F.; Triboulet, R. *J. Electrochem. Soc.* **1979**, *126*, 1868.
(36) Kennedy, J. H.; Frese, K. W. *J. Electrochem. Soc.* **1978**, *125*, 723.
(37) Huda, M. N.; Walsh, A.; Yan, Y. F.; Wei, S. H.; Al-Jassim, M. M. *J. Appl. Phys.* **2010**, *107*, 123712.
(38) *Surface Complexation Modeling*; Lützenkirchen, J., Ed.; Elsevier: Amsterdam, 2006; Vol. 11.
(39) Schoonen, M. A.; Strongin, D. R. In *Environmental Catalysis*; Grassian, V. H., Ed.; Taylor & Francis Group: Boca Raton, FL, 2005; p 37.
(40) Stumm, W. In *Aquatic Chemistry − Interfacial and Interspecies Processes*; Huang, C. P., Omelia, C. R., Morgan, J. J., Eds.; American Chemical Society: Washington, DC, 1995; Vol. 244, p 1.
(41) Stumm, W. *Croat. Chem. Acta* **1997**, *70*, 71.
(42) Royea, W. J.; Fajardo, A. M.; Lewis, N. S. *J. Phys. Chem. B* **1997**, *101*, 11152.
(43) Morrison, R. *Electrochemistry at Semiconductor and Oxidized Metal Electrodes*; Plenum Press: New York, 1980.
(44) Woods, R. In *Modern Aspects of Electrochemistry*; Bockris, J. O., Conway, B. E., White, R. E., Eds.; Plenum Press: New York, 1996; p 401.
(45) Chernyshova, I. V. *J. Electroanal. Chem.* **2003**, *558*, 83.
(46) Chernyshova, I. V. *J. Phys. Chem. B* **2001**, *105*, 8185.
(47) Chernyshova, I. V. *J. Phys. Chem. B* **2001**, *105*, 8178.
(48) Memming, R. *Semiconductor Electrochemistry*; Wiley-VCH: Weinheim, 2001.
(49) Anderman, M.; Kennedy, J. H. In *Semiconductor Electrodes*; Finklea, H. O., Ed.; Elsevier: Amsterdam, 1988; p 146.
(50) Hem, J. D. *Chem. Geol.* **1978**, *21*, 199.
(51) Finklea, H. O. In *Encyclopedia of Electrochemistry*; Bard, A. J., Stratmann, M., Eds.; Wiley-VCH: Weinheim, 2007; Vol. 10, p 623.
(52) McAlpine, N. S.; Fredlein, R. A. *Aust. J. Chem.* **1983**, *36*, 11.
(53) Chen, S. Y.; Gloter, A.; Zobelli, A.; Wang, L.; Chen, C. H.; Colliex, C., *Phys. Rev. B* **2009**, *79*, 104103.
(54) Tian, Y.; Tatsuma, T. *J. Am. Chem. Soc.* **2005**, *127*, 7632.
(55) Fujii, M.; Kawai, T.; Kawai, S. *Chem. Phys. Lett.* **1984**, *106*, 517.
(56) Miyauchi, M.; Nakajima, A.; Watanabe, T.; Hashimoto, K. *Chem. Mater.* **2002**, *14*, 2812.

(57) Fu, Q.; Wagner, T. *Surf. Sci. Rep.* **2007**, *62*, 431.
(58) Liu, X. H.; Zhang, J.; Guo, X. Z.; Wu, S. H.; Wang, S. R. *Nanotechnology* **2010**, *21*, 095501.
(59) Koole, R.; Liljeroth, P.; Donega, C. D.; Vanmaekelbergh, D.; Meijerink, A. *J. Am. Chem. Soc.* **2006**, *128*, 10436.
(60) Williams, A. G. B.; Scherer, M. M. *Environ. Sci. Technol.* **2004**, *38*, 4782.
(61) Yanina, S. V.; Rosso, K. M. *Science* **2008**, *320*, 218.
(62) Rosso, K. M.; Yanina, S. V.; Gorski, C. A.; Larese-Casanova, P.; Scherer, M. M. *Environ. Sci. Technol.* **2010**, *44*, 61.